

# We are IntechOpen, the world's leading publisher of Open Access books Built by scientists, for scientists

6,900

Open access books available

185,000

International authors and editors

200M

Downloads

Our authors are among the

154

Countries delivered to

TOP 1%

most cited scientists

12.2%

Contributors from top 500 universities



WEB OF SCIENCE™

Selection of our books indexed in the Book Citation Index  
in Web of Science™ Core Collection (BKCI)

Interested in publishing with us?  
Contact [book.department@intechopen.com](mailto:book.department@intechopen.com)

Numbers displayed above are based on latest data collected.  
For more information visit [www.intechopen.com](http://www.intechopen.com)



# Earthscraper: A Smart Solution for Developing Future Underground Cities

*Faham Tahmasebinia, Kevin Yu, Jiachen Bao,  
George Chammoun, Edwin Chang, Samad Sepasgozar  
and Fernando Alonso Marroquin*

## Abstract

This chapter reports on the finite element analysis of the “earthscraper,” proposed by BNKR Arquitectura. It was proposed as an alternative building method for the future, as it requires less surface area and lower operating costs than an equivalent aboveground structure. A 2D model of the cross section of the structure was created using Strand7 for steady-state thermal analysis. This solver gave internal temperature ranging between 20 and 38°C between the bottom apex and the surface, respectively. This provides a comfortable temperature by default, displaying the lesser dependency on heating and cooling costs. A 3D model was also created to analyze the effect of lateral earth pressure by the use of the linear static solver. Results give a maximum lateral displacement of 527 mm and 19.8 mm on the exterior and interior walls, respectively. The model was used for earthquake analysis in accordance with AS/NZS1170.4, requiring the natural frequency and spectral response solvers. Twenty-five modal frequencies were found, with 99.6% of the mass of the structure contributing to the direction under analysis. The maximum horizontal displacement of the structure under the designed earthquake loads was found to be 19.2 mm.

**Keywords:** earthscraper, future cities, underground development, numerical modelling, finite element analysis

## 1. Introduction

The United Nations has projected that the world population will reach 9.7 billion by 2050, with the increase of 2.5 billion as to date. The increased pressure on housing solutions to accommodate for the growing population while reducing the carbon footprint has led BNKR Arquitectura [1], based in Mexico City, to formulate a radical solution called the “earthscraper.”

Such a building is an inverted pyramid with the ability to accommodate 100,000 while using a small surface area, allowing easy implementation into developed cities. In addition, its founding into the soil eliminates any wind loading while also ensuring a constant warm temperature imposed by the surrounding soil, reducing the energy consumption for heating and cooling.

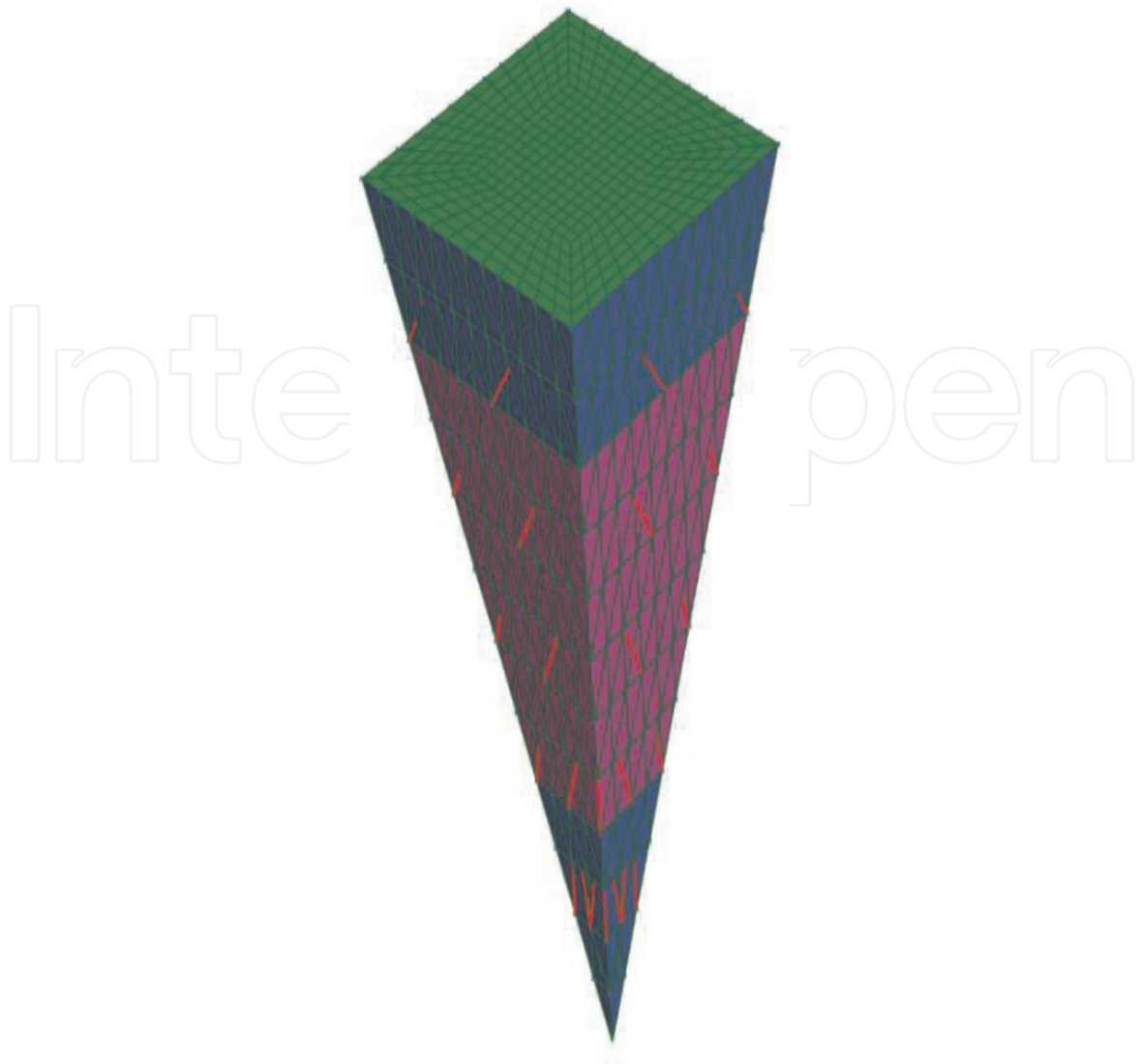


**Figure 1.**  
*Conceptual design of earthscraper.*

The projected populated rise in Sydney is forecast as between 2 million [2], while urban sprawl is limited by the surrounding Blue Mountains, countryside, and ocean [3] (Clarke, 2016). As such, the main objective of this project will investigate the feasibility of implementing the earthscraper in Sydney's geology and climatology. The theoretical loads imposed by earth pressures, thermal loads, and earthquakes loads will be determined, and the structures response will be modeled using Strand7, a finite element method processor.

Post-processing of the results will give the displacement of the building under each respective load, providing an insight into the expected structural performance. The possibility of such a structure as an addition in the future cities of 2050 shall be determined in this chapter (**Figure 1**).

## 2. Structural members

Below is the description of the members of the structure:

Floor system: reinforced concrete one-way floor slabs, 0.3 m thick with N16 reinforcement, sitting on steel beams and acting compositely.

Beams: steel beams of varying length extending from bottom of the exterior wall to the top of the interior wall, interconnected to form a truss system. Steel 360UB44.7 beams supporting the concrete slabs.

Details of the structural elements	Suggested structural element size	Suggested design standards
Steel columns	460UB82.1	AS4100 [4]
Reinforced concrete floor system	40 MPa, thickness 0.3 m, N20 rebars	AS3600 [5]
Reinforced concrete interior wall	40 MPa, thickness 2 m, N20 rebars	AS3600 [5]
Reinforced concrete exterior wall	50 MPa, thickness 2 m, N20 rebars	AS3600 [5]
Truss beams	360UB50.7	AS4100 [4]
Perlucor ceiling	Thickness 0.1 m	AS1288 [6]

**Table 1.**  
*Structural elements.*

Columns: steel UB360.44.7 column spacings at 6.5 m, with floor-to-floor height of 5 m. Steel columns replaced by truss system at locations of intersection.

Walls: reinforced concrete with 1.5–2 m thickness and N20 reinforcement, acting compositely.

Foundation: concrete on rock-concrete pads for columns extruding into the concrete.

Cables: rock bolts to tie back structure.

Ground: water table at 60 m depth, soft soil of unit weight 17 kN/m<sup>3</sup> from depths 0–10 m, and then Hawkesbury sandstone with unit weight 24 kN/m<sup>3</sup> from depths 10–300 m.

Ceiling: perlucor glass ceiling with improved strength and heat insulation compared to normal glass.

Soil: spring dampeners on the exterior of the structure to simulate the soil and the structure’s deformations within the soil.

**Table 1** shows the general element sizes used in the design of the structure. Element sizes were chosen based on design standards and structural strength, combined with numerical analysis to determine the most appropriate member size for the expected loads.

### 3. Structural system

**Figure 2a** shows the dimensions of the structure, with a Perlucor glass ceiling and reinforced concrete walls and a reinforced concrete core running through the center of the structure. The green lines represent the outline of the interior concrete core, the black lines are the outline of the whole structure, the dark blue lines represent the floors, and the light blue lines on the top represent the Perlucor glass.

**Figure 3a** and **b** shows the interior design of the structure for the first level, with the steel cables forming a truss system between the exterior wall and the interior core to provide buckling and bending resistance from the lateral earth pressure loads and earthquake loads.

**Figure 3c** shows the spring dampeners with fixed restraints at the end away from the wall and free restraints at the connection with the wall to simulate the behavior of the structure within the soil mass.

The concrete floor slabs use N16 reinforcement bars at a spacing of 100 mm, while the reinforced concrete wall and core use N20 reinforcement bars at a spacing of 100 mm. The reinforcement helps the structure resist tensile loads due to the large bending moments caused by the lateral earth pressure.

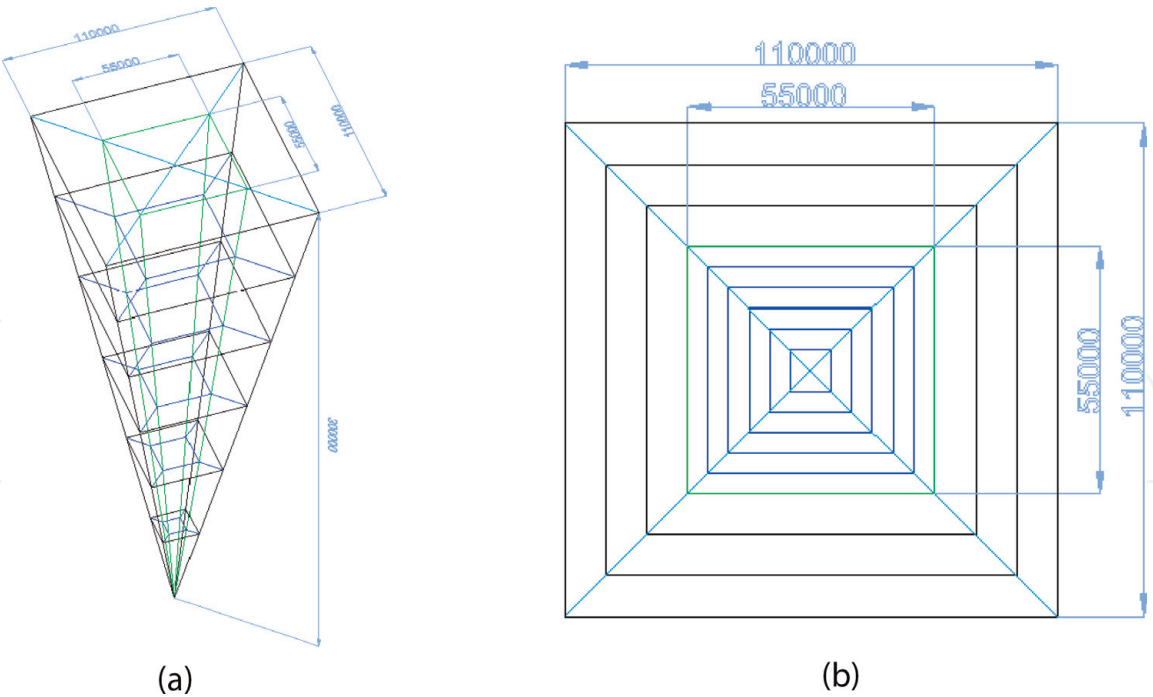


**Figure 2.**  
(a) CAD rotated section view of entire structure and (b) CAD plan view from ground level.

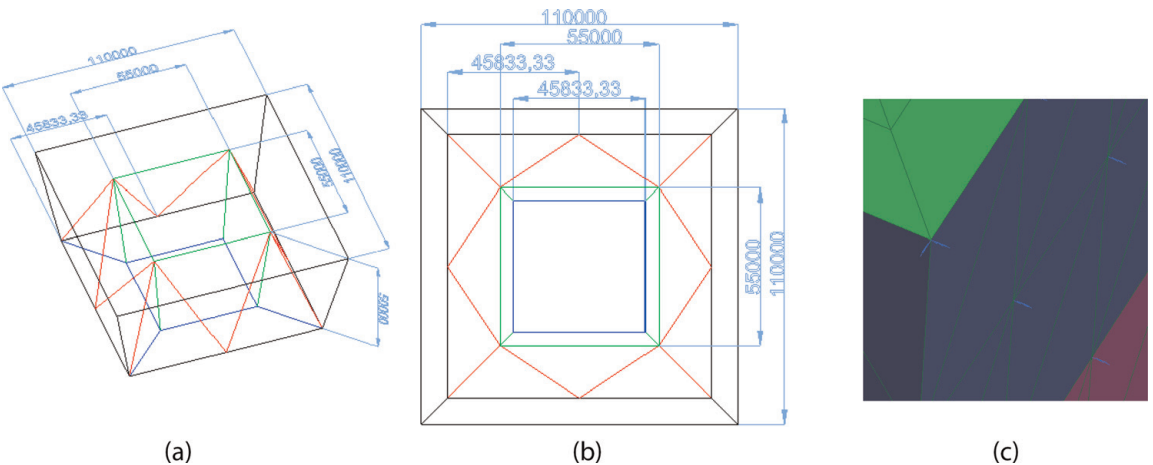


**Figure 3.**  
(a) CAD section view of first level, (b) CAD plan view of first level and (c) spring dampeners.

The system resists vertical loads through load transfer from the roof and floor slabs into the columns, through the beams and truss system. The vertical loads within the columns are then transferred into the surrounding sandstone. The beams and columns of each individual floor have been omitted from the design, and the 60 floors of the 300 m deep structure have been simplified to 6 floors, as the vertical loads are not the focus of this structural design, since the surrounding Hawkesbury sandstone will be able to withstand the dead and live loading of the structure.

The system resists lateral loads with the truss system and floor slabs acting as struts, reducing the overall deflection of the structure and distributing lateral loads throughout the floor and into the surrounding bedrock. The floors resist loads by transferring vertical live and dead loads into the support steel beams, and the slabs resist lateral loads by transferring the loads either into the interior wall or exterior wall. The beams resist loads by transferring horizontal and vertical loads into nearby columns or walls. In addition, the beam truss elements provide different load paths and brace the structure to further reduce the stress concentrations on members. The columns resist load by transferring horizontal and vertical loads into the base pads and then into the surrounding bedrock.



Since the structure and its 50 floors are very complex to design for using Australian design codes, it was simplified into 6 larger floors to consider overall trends of stresses and deflections. This was done to locate areas of significant stresses and deflection and where the structure is most likely to fail. Strategies were then implemented to counteract these problem areas, such as increasing wall thickness or concrete strength.

## 4. Loads

### 4.1 Lateral earth loads (earth pressure)

The loads imposed onto the earthscraper by the surrounding soil and water were calculated using effective earth pressures, which are shown below and expanded in Appendix A:

$$\sigma'_h(z) = K_0 \sigma'_v(z), \tag{1}$$

$$K_0 = 1 - \sin(\phi), \tag{2}$$

Eq. (1) shows the relationship between vertical effective pressure and lateral earth pressure through the at-rest coefficient of earth pressure,  $K_0$ . Eq. (2) gives an expression for  $K_0$ , given by Jaky [7] as a function of the internal friction angle  $\phi$ . These lateral earth pressures act on the exterior wall, causing horizontal deflection of external and internal wall after load transfer.

**Figure 4** shows the lateral pressures varying linearly, with a change in gradient at 10 m depth with the change from soft soil to Hawkesbury sandstone. At a depth of 60 m is the water table, introducing pore water pressures and increasing the lateral loading on the structure. This representation of earth pressures.

### 4.2 Thermal loads

The thermal loads imposed onto the structure include the solar heat flux, the convection currents between the structure and outside fluid, and the external ambient pressure of the surface. The ambient temperature surrounding the earthscraper was determined through research of past studies. The topsoil temperature was averaged across 1980–2006 for the top 20 cm, determined as 19.65°C [8].

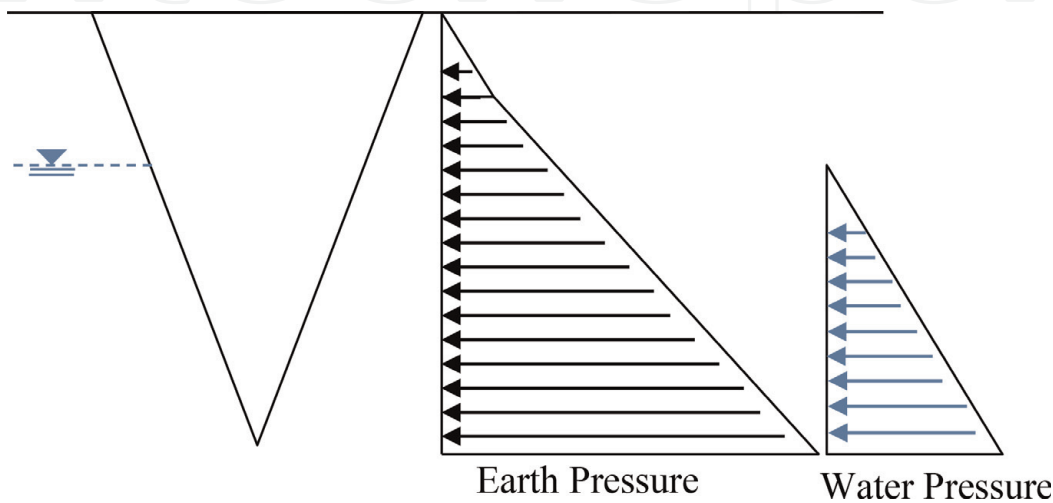


**Figure 4.**  
Vertical profile of lateral earth pressure—a combination of soil pressure and water pressure.

The temperature of the soil is taken to linearly increase with depth, with a determined thermal gradient of  $0.07^{\circ}\text{C}/\text{m}$ .

The ambient temperature of the surface was chosen as the mean temperature at the Sydney Observatory Hill Bureau Weather Station since 1859, determined as  $22.1^{\circ}\text{C}$  [8]. However, due to the incoming solar radiation, the heat flux also contributes to the heat transfer to the Perlucor ceiling. Calculations for an absorbing black-body give a heat flux of  $1.37\text{ kW}/\text{m}^2$ ; however, due to cloud albedo, atmospheric absorption, and radiation reflection, the solar exposure is taken as  $69.44\text{ W}/\text{m}^2$  [8].

### 4.3 Earthquake loads

The response of the structure under earthquake loads requires the use of dynamic analysis, as the earthscraper falls into the earthquake design category III (EDCIII), as determined in Appendix C. This method shall comply with AS/NZS1170.4 [9] Section 7 with the use of a modal response spectrum analysis.

## 5. Structural design

The initial analysis was undertaken with all concrete wall elements and floors as the same plain concrete with 40 MPa strength and 0.5 m wall thickness. Upon linear static and spectral analysis, it was found that horizontal deflections along the second, third, and fourth floors were much greater than the first, fifth, and sixth floors. As a response, concrete reinforcement was added throughout the structure to better resist the lateral loads, and the concrete wall thickness was increased to 2 m for the second, third, and fourth floors. In addition, the concrete strength used was increased to 50 MPa for the second, third, and fourth floors. The first, fifth, and sixth floors were also increased in wall thickness to 1.5 m.

To further combat the deflections and stresses found within the structure, a steel beam truss system was created to connect the exterior wall to the interior wall, providing additional strutting and load transfer throughout the structure. 360UB44.7 beams were chosen for their relative light weight and strength. Perlucor glass was chosen for the ceiling design for its superior strength and thermal properties compared to standard glass and to fulfill the need to have a transparent ceiling material for light transfer downwards into the structure.

## 6. Strand7 models

### 6.1 2D model

A two-dimensional model was created to model the temperature within the structure. A quad 4 plate was created with the thermal properties of air and the dimensions of a vertical cut through the middle of the structure. The structure was then subdivided, and the top layer of plates was changed to the structural properties of glass with the thermal properties of Perlucor. The sidewalls were then converted to the structural and thermal properties of concrete (Figure 5).

### 6.2 3D model

The model was formed by creating tri-3 elements as the exterior and interior walls. The floors and ceiling were then created using quad 4 elements. The truss

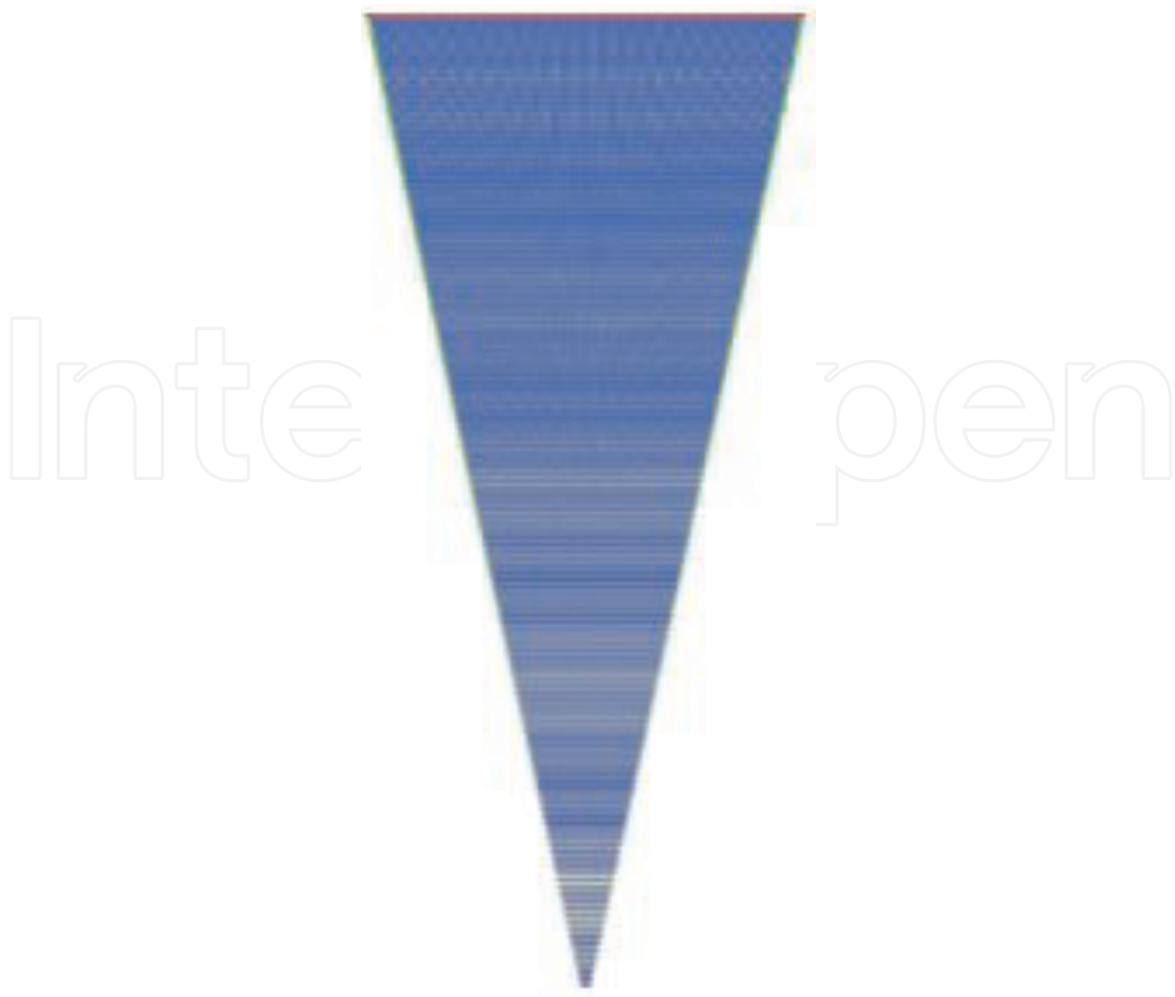


**Figure 5.**  
*2D model of the earthscraper created using Strand7 cross section showing the perlucor ceiling (red), green concrete exterior walls (green), and the air inside (blue).*

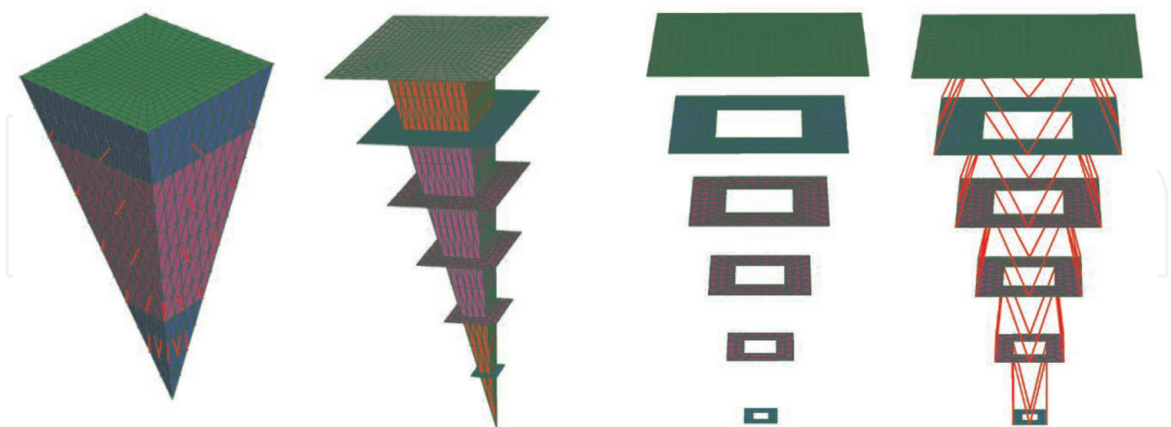


**Figure 6.**  
*Stages of 3D model creation—exterior walls, interior walls and floors, and beam truss (from left to right).*

beams were then made using beam 2 elements. Each element type was then separated into six groups for their respective floors. The plate elements were then subdivided. Finally, spring dampener beam 2 elements were created by selecting the nodes on each face of the structure and then extruding by increment of 1 m in the negative Z direction or the face's equivalent axis perpendicular to the vertical axis pointing outward. Fixed conditions were then applied to the base node of the



structure (tip of the pyramid), as well as the node of the spring dampeners not attached to the structure (Figure 6).

7. Numerical analysis

7.1 Thermal analysis

The transfer of thermal energy occurs in two thermal paths. The Perlucor ceiling at the surface ambient temperature absorbs the solar radiation, transporting the heat internally through conduction and heating the internal air through convection. In addition, the walls of the structure also at the ambient temperature of the surrounding soil conduct this energy through the wall system and expel this energy through convection within the structure.

An ambient temperature of 22.1°C was applied at the top surface, and the linearly increasing ambient temperature of the soil was applied along the sidewalls. A convection coefficient of 11 and 23 W/mK was applied along the Perlucor ceiling and sidewall, respectively, and heat flux from the sun of 69.44 W/m<sup>2</sup> was applied along the top surface. The results of the static thermal solver are shown below, alongside the model used.

Figure 7 shows a maximum temperature of 38°C at the bottom vertex, a region designed to harness geothermal energy. This, however, will not be sufficient for energy production according to the thermal analysis. Otherwise, the building reaches thermal equilibrium at comfortable temperatures. Ranging between 19 and 25°C for the upper third of the structure almost eliminates the need for cooling or heating costs. Although the lower section exceeds standard room temperature (25°C), the cooling costs would be lower compared to a standard aboveground structures.

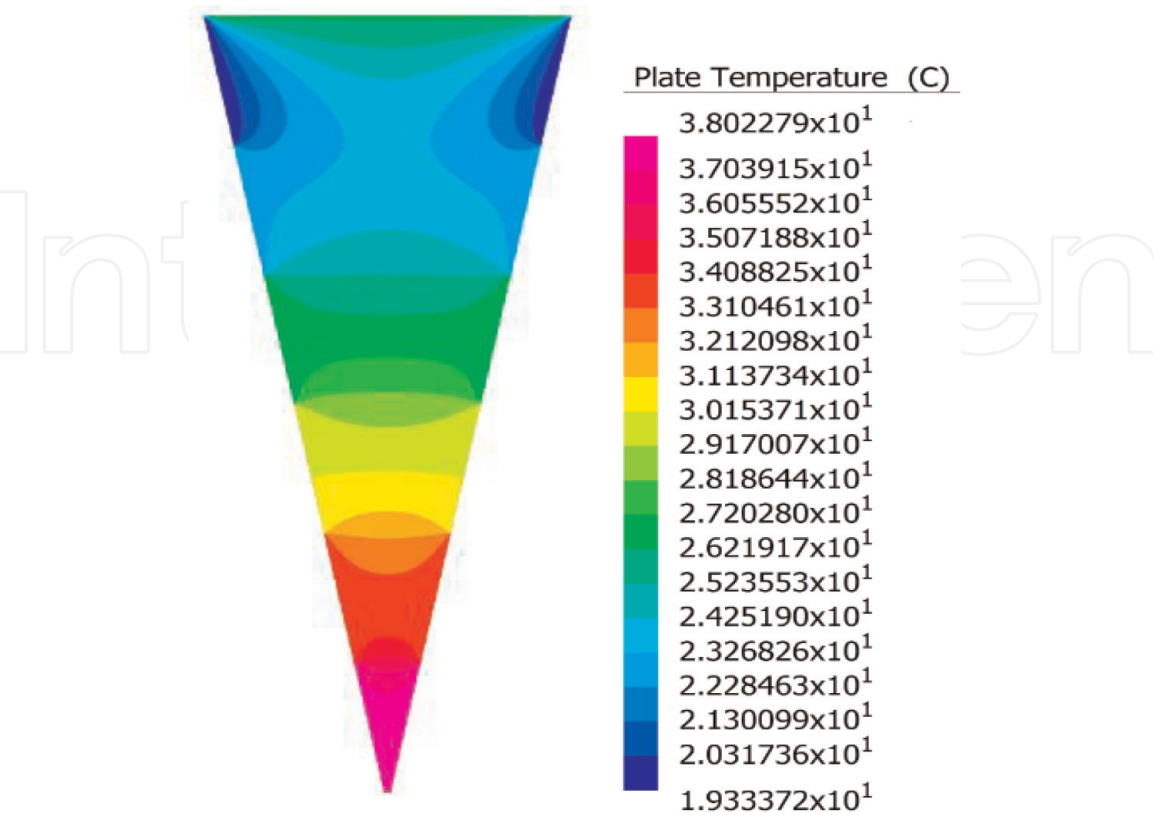


Figure 7.  
Temperature contour of steady-state heat solver.

## 7.2 Earth pressure analysis

### 7.2.1 Linear static solver

The 3D model shown in **Figure 6** was used to analyze the horizontal displacement of the earthscraper under lateral earth pressures. To achieve this, the model was run under the linear static solver, with the following results produced. **Figure 8** portrays the horizontal displacements under lateral earth pressures. The internal walls experience a maximum deflection of 28 mm, whereas the external walls experience 527 mm of deflection.

### 7.3 Earthquake analysis

Dynamic analysis can be used to calculate the response under earthquake loading. The acceleration vector,  $\ddot{U}$ , and displacement vector,  $U$ , of a structure under the action of a time-dependent force,  $F(t)$ , are given by the matrix element equation:

$$M\ddot{U} + KU = F(t), \tag{3}$$

where  $M$  is the mass matrix and  $K$  is the stiffness matrix of the structure in Eq. (3). This can be solved using the transient solver; however, it is quite computationally demanding. Alternatively, the Strand7's spectral response solver coupled with the natural frequency solver can be used to determine the structure response under an external loading.

#### 7.3.1 Natural frequency solver

The natural frequencies of the structure can be found by removing the external and damping forces and introducing an oscillatory function,  $U(t)$ , shown below in Eq. (4). This yields the characteristic equation showed in Eq. (5):

$$U(t) = U_0 e^{j\omega t}, \tag{4}$$

$$|K - \omega^2 M| = 0, \tag{5}$$

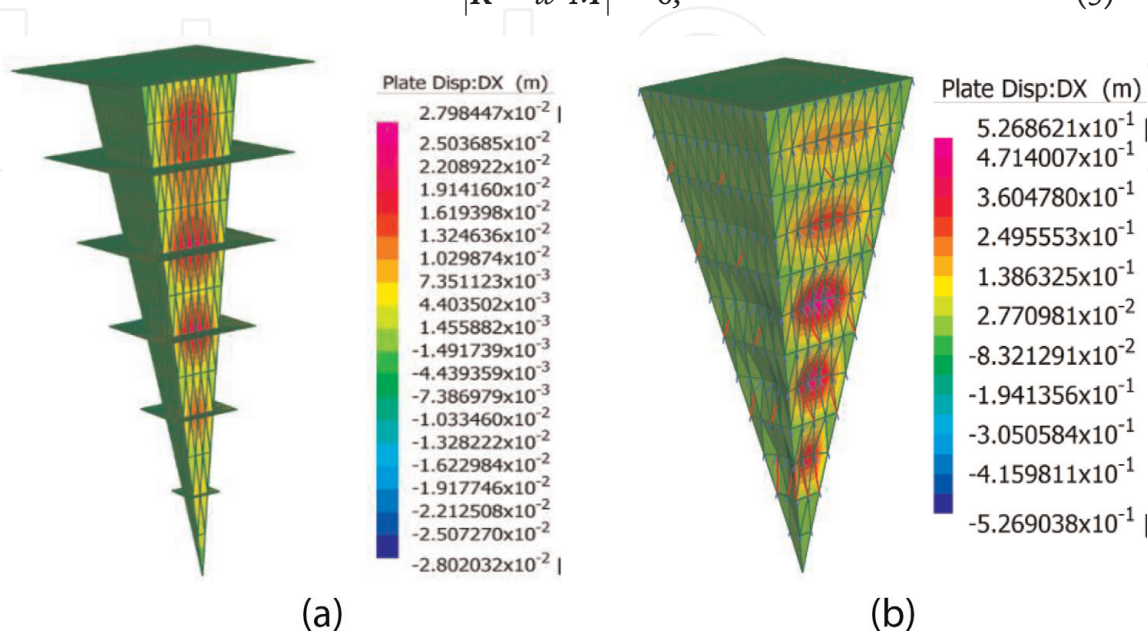


**Figure 8.**  
(a) Interior deflection contour and (b) exterior deflection contour.

Mode	Frequency (Hz)	Mode	Frequency (Hz)	Mode	Frequency (Hz)	Mode	Frequency (Hz)	Mode	Frequency (Hz)
1	0.0933	6	0.5729	11	0.7063	16	0.7847	21	0.8881
2	0.0983	7	0.5829	12	0.7144	17	0.7847	22	0.8882
3	0.0986	8	0.5829	13	0.7144	18	0.8305	23	0.9295
4	0.2818	9	0.5829	14	0.7342	19	0.8312	24	0.9295
5	0.5729	10	0.5830	15	0.7473	20	0.8673	25	0.9960

**Table 2.**  
*Frequency and modes of the natural frequency solver.*

where  $w$  is the natural frequency and the solution gives a polynomial function of  $w^2$  with order equal to the degrees of freedom of the structure. The number of degrees of freedom equals to the number of modes, and the modal shapes are found by normalizing the vibrational modes, shown below in Eq. (6):

$$U_i^T M U_i = 1, \tag{6}$$

The natural frequency solver uses this method to find the modal shapes and the respective frequency,  $w_i$ , with the modes and respective frequencies found tabulated below. This is as specified by Clause 7.4, with 25 modes found to have converged. **Table 2** shows the different modes and their respective frequencies.

7.3.2 Spectral response solver

The method of spectral response involves determining the peak response of the structure due to an applied acceleration, which is given by the acceleration response shown in Eq. (7):

$$S_a(w_i) = |\ddot{S}(t)|_{max}, \tag{7}$$

$$S_i(t) = \int_0^t g(\tau) \frac{\sin(w(t-\tau))}{w} d\tau, \tag{8}$$

The spectral response acceleration was input into Strand7 in compliance with AS/NZS1170.4 Clause 7.2, in which the horizontal design spectrum,  $C_d(T)$ , was determined and is plotted in **Figure 9**.

The maximum displacement is then found by method of square root of the sum of the squares (SRSS) satisfying Clause 7.4.3, in which the contribution of each mode is superposed such that

$$U_{max} = \sqrt{\sum_{i=1}^{n_{dof}} \phi_{i,max}^2}, \tag{9}$$

$$\phi_{i,max} = \Gamma_i S(w_i), \tag{10}$$

where  $\Gamma_i$  is the mass participation factor, a measure of the contribution of mode  $i$ . A detailed explanation is given in Appendix C. The displacement contour was plotted using the SRSS method. It is shown in **Figure 10** that the maximum displacement due to earthquake loads is 19.8 mm, insignificant relative to the scale of the structure. It should be noted, however, that the design standard AS1170.4 [6] used to generate the numerical analysis does not account for liquefaction,

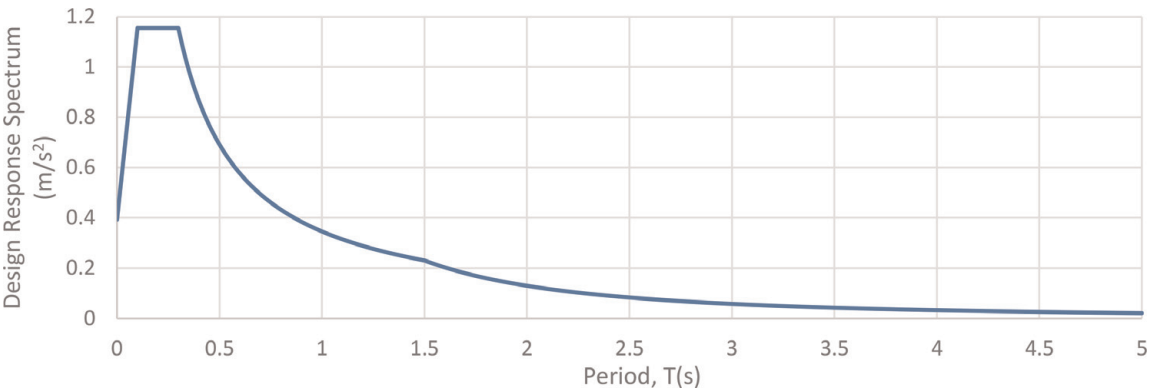


**Figure 9.**  
Design response spectrum.

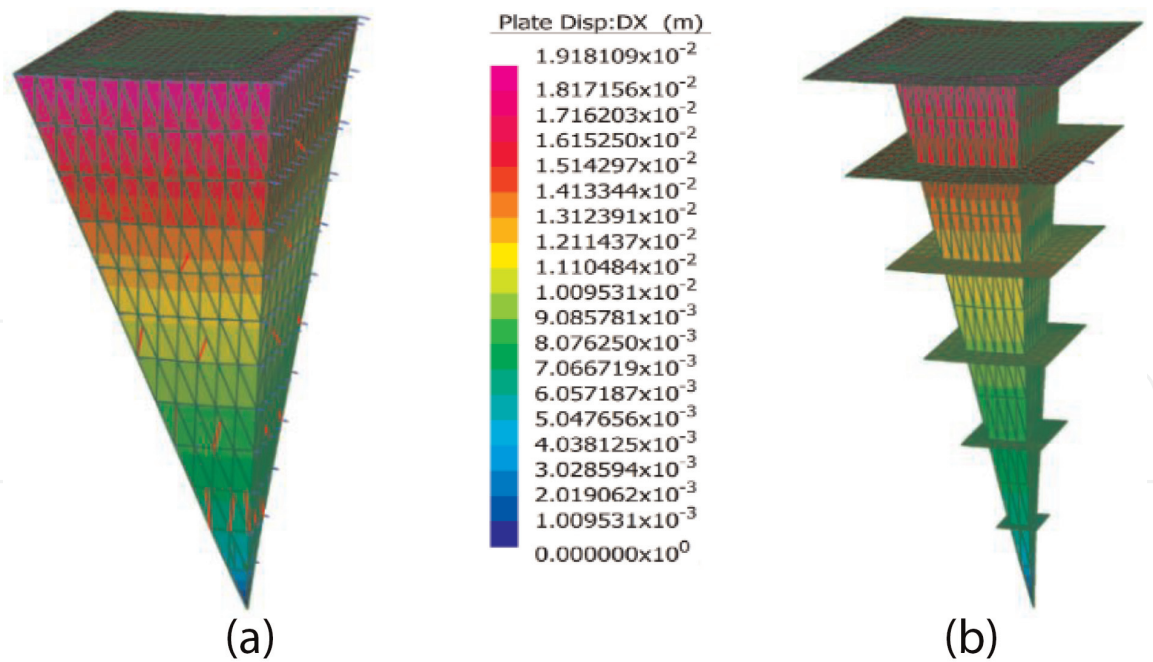


**Figure 10.**  
(a) Exterior deflection under earthquake loads and (b) internal deflection under earthquake loads.

settlement, or fault rupture effects on the soil and as such may be underestimating the effects of earthquake loads on underground structures.

## 8. Conclusions

This chapter provides a 3D linear static and spectral analysis, as well as a 2D thermal analysis of an inverted pyramid structure modeled off the architectural design of the firm BNKR Arquitectura [8].

Both the 2D and 3D models have been successful in determining the loading conditions of the structure, as well as identifying key structural areas of increased stress, deflection, and heat. Using this analysis, modifications to the structure were made to reduce the effect of these loads and bring the structure within an acceptable level. A final design with a simplified six-floor system arrived upon to allow a sufficiently accurate model while maintaining the viability of 3D modeling within the finite element analysis software Strand7.

While the results found are encouraging, further research should be undertaken to investigate the liquefaction effect of earthquake loads on underground structures and soil. In addition, more detailed structural modeling could be undertaken to investigate the minutia of detail for each individual story, rather than simplifying into six larger general floors.

Therefore, the structure could feasibly be considered in 2050, with a rapidly increasing sophistication of software and material engineering. The demands of the human population in 30 years may necessitate such an ambitious design.

## Appendices

### A. Earth pressure analysis

**Figure 11** portrays the soil pressures experienced by the external walls of the structure, with the relevant values kept parametrized for the determination of Eq. (10).



For substitution in Eq. (10), the parameters and their respective values are shown in **Table 3**. These values were found through literature review and govern the lateral earth pressures experienced by the structure.

The lateral pressure is given as

$$\sigma_h(z) = \sigma'_h(z) + u(z), \tag{11}$$

where  $u(z)$  is the pore water pressure, given as the hydrostatic water pressure shown below

$$u(z) = \gamma_w \langle z - d_w \rangle, \tag{12}$$

and  $\sigma'_h(z)$  is the effective lateral pressure, expressed as

$$\sigma'_h(z) = K_0 \sigma'_v(z), \tag{13}$$

where  $K_0$  is the coefficient of earth pressure at rest, given by the following expression given by Jaky [7]

$$K_0 = 1 - \sin(\phi), \tag{14}$$

and  $\sigma'_v(z)$  is the effective vertical earth pressure. This is the contribution of the different soil layers less the effect of pore water pressure, given as

$$\sigma'_v(z) = \gamma_{ss}(z - \langle z + d_{ss} \rangle) + \gamma_{hs} \langle z - d_{ss} \rangle - \gamma_w \langle z - d_w \rangle, \tag{15}$$

The Macaulay brackets seen above operate as follows:

$$\langle z - a \rangle^n = \begin{cases} 0, & z < a \\ (z - a)^n, & z \geq a \end{cases}, \tag{16}$$

This allows one expression for earth pressure at any depth. Replacing all the relations together gives

$$\sigma_h(z) = K_0(\gamma_{ss}(z - \langle z + d_{ss} \rangle) + \gamma_{hs} \langle z - d_{ss} \rangle) + (1 - K_0)\gamma_w \langle z - d_w \rangle, \tag{17}$$

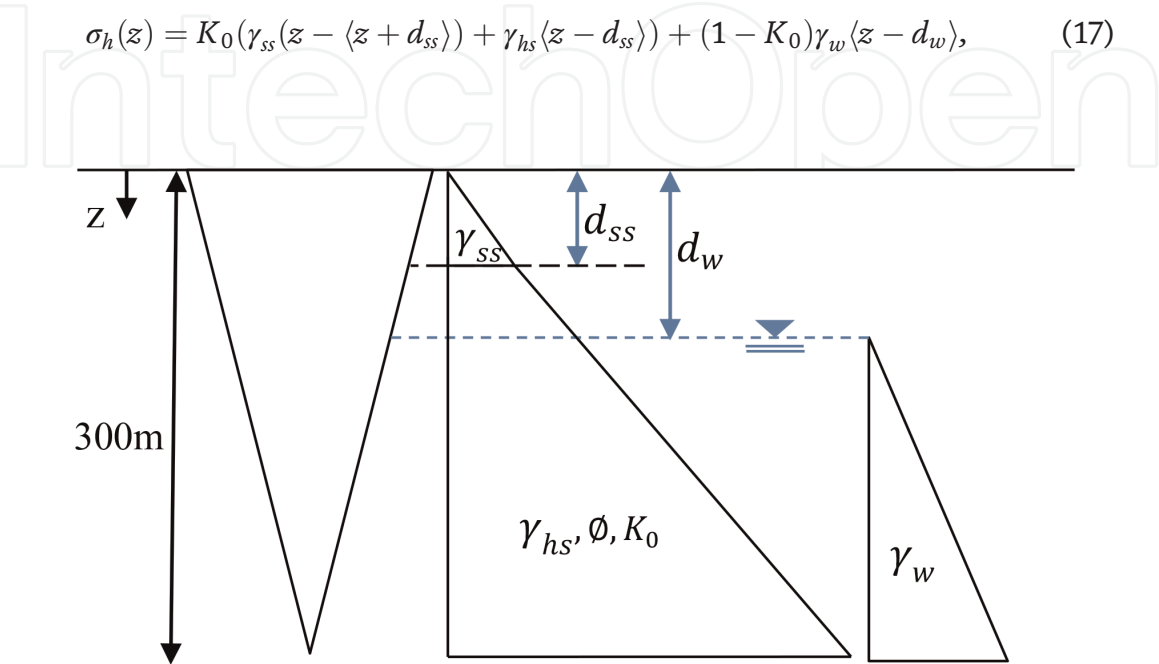


**Figure 11.**  
 Earth pressure profile.

Parameter	Value
Internal friction angle, $\phi(^{\circ})$	47.2
At-rest coefficient of earth pressure, $K_0$	0.26627
Soft soil unit weight, $\gamma_{ss}$ (kN/m <sup>3</sup> )	17
Water unit weight, $\gamma_w$ (kN/m <sup>3</sup> )	10
Hawkesbury sandstone unit weight, $\gamma_{hs}$ (kN/m <sup>3</sup> )	24
Depth of soft soil, $d_{ss}$ (m)	10
Depth of water table, $d_w$ (m)	60

**Table 3.**  
*Earth pressure parameters.*

At the bottom of the structure, i.e.,  $z = 300$  m, the lateral earth pressure is calculated as 3.66 MPa, shown below in Eq. (10) using the parameters in **Table 3**:

$$\sigma_h(300) = 0.26627(17(10) + 24(300 - 10)) + (1 - 0.26627)10(300 - 60) = 3.66 \text{ MPa} \tag{18}$$

**B. Thermal analysis**

The thermal properties of the materials used in the structure are given in **Table 4**. These parameters determine the conductivity and transfer of heat throughout the structure. The reinforced concrete conducts a relatively higher amount of heat compared to the Perlucor ceiling, both absorbing external heat from the soil and surface, respectively.

The heat flux on the Perlucor ceiling can be estimated for a blackbody using Stefan-Boltzmann law. The heat flux generated at the sun’s surface,  $q_{sun}$ , is given by

$$q_{sun} = \epsilon\sigma(T_{sun}^4 - T_{space}^4), \tag{19}$$

Hence, for radius,  $R$ , of the sun and distance  $D$  from the sun to the earth, the heat flux experienced by earth is

$$q_{earth} = \epsilon\sigma(T_{sun}^4 - T_{space}^4)\left(\frac{R}{D}\right)^2, \tag{20}$$

The parameters needed for Eq. (17) are shown in **Table 5**, giving the value of

$$q_{earth} = 1 \times 5.67 \times 10^{-8}(5780^4 - 3^4)\left(\frac{6.957 \times 10^5}{1.5 \times 10^8}\right)^2 = 1.361 \frac{\text{kW}}{\text{m}^2}, \tag{21}$$

Material	Reinforced concrete	Perlucor	Air
Coefficient of thermal energy (W/m K)	1.37	0.78	0.0257
Specific heat capacity (J/kg K)	880	840	1005

**Table 4.**  
*Material thermal properties.*

Parameter	Value
Stefan – Boltzmann constant, $\sigma$ ( $\text{W}/\text{m}^2 \text{K}^4$ )	$5.67 \times 10^{-8}$
Temperature of Sun, $T_{\text{sun}}$ (K)	5780
Temperature of space, $T_{\text{space}}$ (K)	3
Distance from sun, $D$ (km)	$1.5 \times 10^8$
Radius of sun, $R$ (km)	$6.957 \times 10^5$
Radiation coefficient of sun, $\epsilon$	1

**Table 5.**  
Heat flux parameters.

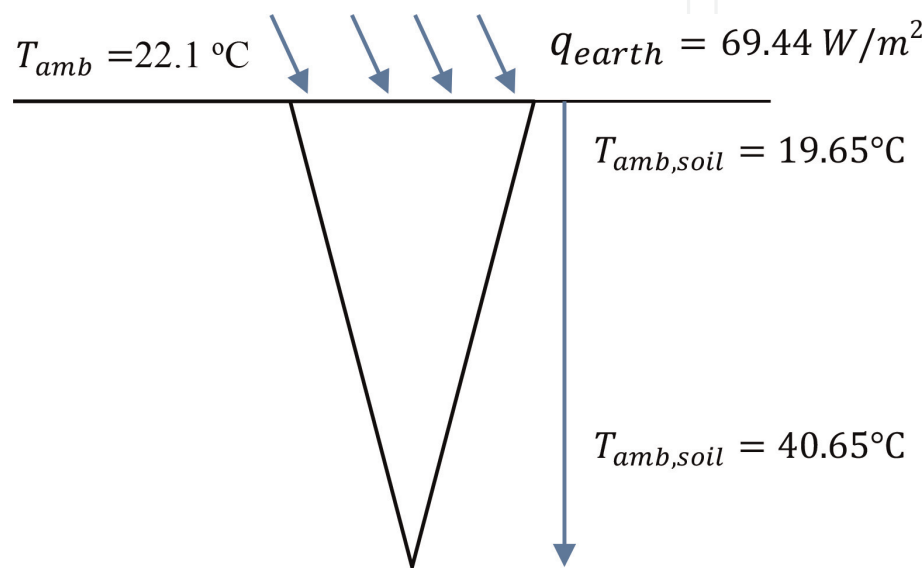


**Figure 12.**  
Thermal conditions.

This however assumes the earth acts as a blackbody, absorbing all incoming radiation. Measurements by the Bureau of Meteorology have shown that the incoming solar radiation is of the value of  $69.44 \text{ W}/\text{m}^2$ , significantly lesser than the blackbody value. This is due to solar irradiance, cloud reflection, atmospheric absorbance, and the reflection of the earth surface. The thermal boundary conditions are shown in **Figure 12**.

### C. Earthquake analysis

Pells (2004) determined the bearing capacity of Hawkesbury sandstone as 20–103 MPa and 6–14 MPa for laboratory tests and field tests, respectively. Taking the field tests as true, this classifies the rock as subsoil Class B<sub>e</sub> (AS/ZS1170.4 Clause 4.2.2).

Using AS/NZS1170.4, the hazard factor, Z, in Sydney is 0.08. For an important factor of 3 (BCA 2016), the structure has an annual probability of exceedance of 1/1000 (BCA 2016).

AS/NZS1170.4 gives the probability factor of 1.3 for an annual probability of exceedance of 1/1000.

AS/NZS1170.4, for a structure height of 300 m, the earthquake design category is EDCIII. Structural ductility factor ( $\mu$ ) and structural performance factor ( $S_p$ ) are found as 2 and 0.77, respectively (AS/NZS1170.4).

The spectral shape factor,  $C_h(T)$ , is found by using AS/NZS1170.4 Clause 6.4. This requires the period of vibration of the structure, which was found using the natural frequency solver. The horizontal design response spectrum,  $C_d(T)$ , is found using AS/NZS1170.4 Clause 7.2, given as

$$C_d(T) = k_p Z \frac{S_p}{\mu} C_h(T) = 1.3 \times 0.08 \times \frac{0.77}{2} C_h(T) = 0.04004 C_h(T), \quad (22)$$

The scaling factor is multiplied by the gravitational acceleration to give the horizontal acceleration in terms of  $\text{m/s}^2$ . This process is summarized in **Table 6**, showing the modes, the respective frequency and period, then the calculated and design spectral response factor, and then the mass participation factor. The total mass participation of the 25 nodes is 99.461%, satisfying AS/NZS1170.4 Clause 7.4.2.

Mode	Frequency (Hz)	Period (s)	$C_h(T)$	$C_d(T)$ (g)	$C_d(T)$ ( $\text{m/s}^2$ )	$\Gamma_i$ (%)
1	0.0933	10.7209466	0.011484383	0.000459835	0.004510978	0.516
2	0.0983	10.1726597	0.012755718	0.000510739	0.005010349	88.177
3	0.0986	10.1378712	0.012843411	0.00051425	0.005044794	0
4	0.2818	3.5484392	0.104833282	0.004197525	0.041177716	0
5	0.5729	1.7455268	0.433232339	0.017346623	0.17017037	0.001
6	0.5729	1.7455268	0.43323234	0.017346623	0.170170371	0
7	0.5829	1.7156367	0.448459526	0.017956319	0.176151493	0
8	0.5829	1.7155891	0.448484434	0.017957317	0.176161277	0.019
9	0.5829	1.7155890	0.448484477	0.017957318	0.176161294	0
10	0.5830	1.7154045	0.448580981	0.017961182	0.1761992	0
11	0.7063	1.4159108	0.621508079	0.024885183	0.24412365	0
12	0.7144	1.3998054	0.628658824	0.025171499	0.246932408	0.018
13	0.7144	1.3998053	0.628658855	0.025171501	0.24693242	0
14	0.7342	1.3620201	0.646099116	0.025869809	0.253782822	0
15	0.7473	1.3381278	0.657635248	0.026331715	0.258314127	0
16	0.7847	1.2744305	0.690504491	0.0276478	0.271224916	0.007
17	0.7847	1.2744305	0.690504508	0.027647801	0.271224923	0
18	0.8305	1.2041558	0.730802435	0.029261329	0.287053642	0
19	0.8312	1.2031179	0.731432875	0.029286572	0.287301275	0
20	0.8673	1.1530177	0.763214655	0.030559115	0.299784916	0
21	0.8881	1.1259461	0.781564952	0.031293861	0.306992773	10.722
22	0.8882	1.1259172	0.781585013	0.031294664	0.307000653	0
23	0.9295	1.0758671	0.81794486	0.032750512	0.321282524	0
24	0.9295	1.0758671	0.817944861	0.032750512	0.321282525	0
25	0.9960	1.0040134	0.876482347	0.035094353	0.344275605	0

**Table 6.**  
Natural frequency results and spectral response.

IntechOpen

## Author details


Faham Tahmasebinia<sup>1,2\*</sup>, Kevin Yu<sup>1</sup>, Jiachen Bao<sup>1</sup>, George Chammoun<sup>1</sup>,  
Edwin Chang<sup>1</sup>, Samad Sepasgozar<sup>2</sup> and Fernando Alonso Marroquin<sup>1</sup>

<sup>1</sup> School of Civil Engineering, The University of Sydney, Sydney, NSW, Australia

<sup>2</sup> Faculty of Built Environment, The University of New South Wales, Sydney,  
NSW, Australia

\*Address all correspondence to: [faham.tahmasebinia@sydney.edu.au](mailto:faham.tahmasebinia@sydney.edu.au)

## IntechOpen

© 2020 The Author(s). Licensee IntechOpen. This chapter is distributed under the terms  
Commons Attribution - NonCommercial 4.0 License (<https://creativecommons.org/licenses/by-nc/4.0/>), which permits use, distribution and reproduction for  
non-commercial purposes, provided the original is properly cited. 



## **References**

- [1] Sol Robles J. La Redención del Ornamento: Recuperando la Dimensión Simbólica de la Arquitectura. *RevistArquis*. 2012;**1**(2):26-35
- [2] McDonald P, Kippen R. Projecting future migration levels: Should rates or numbers be used? *People and Place*. 2002;**10**:82-83
- [3] Morse JM et al. Developing Grounded Theory: The Second Generation. New York: Routledge; 2016
- [4] Trahair N, Bradford MA. Behaviour and Design of Steel Structures to AS4100: Australian. New York: CRC Press; 2014
- [5] Gilbert R. Creep and shrinkage models for high strength concrete—Proposals for inclusion in AS3600. *Australian Journal of Structural Engineering*. 2002;**4**(2):95-106
- [6] AS AS. Glass in Buildings-Selection and Installation. Standards Association of Australia. 1989
- [7] Jaky J. Pressure in silos. In: *Proceedings of 2nd ICSM*. Japan: ICSM; 1948
- [8] Hudson D et al. ACCESS-S1: The new Bureau of Meteorology multi-week to seasonal prediction system. *Journal of Southern Hemisphere Earth Systems Science*. 2017;**67**(3):132-159
- [9] Sharma R, Richards P. The influence of Helmholtz resonance on internal pressures in a low-rise building. *Journal of Wind Engineering and Industrial Aerodynamics*. 2003;**91**(6):807-828